Original Research Article

Research on Cross-scale Micro-gripper Based on Multi-stable Flexible Mechanism

GUAN Miao

School of Mechanical Engineering，Xi'an Technological University，Xi'an 710021，China

Abstract: In order to solve the problems of low precision, small stroke, and inabilityto grip objects across scales (um-mm) in traditional micro-gripper, a multi-stable flexible mechanism-based cross-scale micro-gripper structure was proposed. The multi-stable structure is combined with the traditional amplifying mechanism. The leftside of the micro -gripper adopts a lever mechanism and a parallelogram mechanism, and the right side adopts three different bistables in series to achieve eight-stable state. Finally, the parallelogram mechanism ensures the end of the micro-gripper. The output is pure parallel movement. Firstly, the overall structure design of the micro-gripper is introduced; secondly, the displacement amplification ratio and multi -stable characteristics of the amplification mechanism are deduced through theoretical calculation; finally, the performance and reliability of the micro-gripper are verified by the simulation analysis of the model by finite element. The micro-gripper has high magnification, large grippering range, compact structure, and can realize parallel grippering across μm-mm.

Keywords: Micro-gripper; Compliant multi-stable mechanism; Lever-amplifying mechanism; Cross-scale; Finite element analysis.

1. Introduction

With the rapid development of microelectronics and micro nano technology, fields such as Microelectromechanical Systems (MEMS), micro assembly, and biomedical research have become hot topics both domestically and internationally[1]. Microgripper, as the end effector of micro assembly systems, directly connect the operating mechanism with micro parts and play a decisive role in the manufacturing and assembly of micro parts[2].

The main function of microgripper is to grasp or clamp small parts and components. For small devices that need to be operated, their sizes range from micrometers to millimeters. The displacement resolution of micro gripper drivers is high, but the driving displacement is small. Therefore, the small displacement output by the driver is often amplified by a compliant mechanism and then transmitted to the jaws[3]. Compared to traditional mechanical amplification mechanisms, bistable and multi-stable compliant mechanisms have advantages such as simple structure, easy fabrication, high accuracy, and low friction and wear during motion[4]. Therefore, this article is based on the design of microgripper using multi steady state flexible mechanisms.

The main function of micro grippers is to grasp or clamp small parts and components. For small devices that need to be operated, their sizes range from micrometers to millimeters. The displacement resolution of micro gripper drivers is high, but the driving displacement is small. Therefore, the small displacement output by the driver is often amplified by a compliant mechanism and then transmitted to the jaws. Compared to traditional mechanical amplification mechanisms, bistable and multi-stable compliant mechanisms have advantages such as simple structure, easy fabrication, high accuracy, and low friction and wear during motion. Therefore, this article is based on the design of micro grippers using multi steady state flexible mechanisms.

Scholars at home and abroad have conducted extensive research on expanding the clamping stroke of micro

Received: 9 April 2022 Accepted: 28 April 2022 Available online: 19 May 2022

clamps, mainly through flexible displacement amplification mechanisms. The commonly used micro displacement amplification mechanisms include lever amplification mechanisms, bridge amplification mechanisms, and Scott amplification mechanisms. Li Jiajie et al[5]. designed a new two-stage differential lever micro displacement amplification mechanism. After optimization, the displacement amplification factor of the mechanism was 48, but the error between the finite element simulation model and the theoretical model was 8%. Zhao et al[6]. designed a piezoelectric driven three-level amplification micro gripper with an amplification factor of 16.8 times and an output stroke of only 102.3 μ M. Ding Yan et al[7]. designed a new type of two-stage amplification flexible micro clamp structure, with a displacement amplification ratio of 30.89 and a single gripper stroke of only 334.01 μ M. Chen Xiaodong et al[8]. designed a large stroke two-stage displacement amplification flexible piezoelectric micro clamp. When there is no clamping object, the unilateral output displacement is 237.82 μ m. The actual magnification is 23.782 times. However, the above micro clamps cannot simultaneously hold objects at the micrometer and millimeter levels. Therefore, it is necessary to develop micro clamps with good universality and suitable for cross scale micro operations.

2. Design of Micro Clamp Structure

Figure 1 shows the structure diagram of the micro clamp, with an overall size of 6.04mm × 4.58mm × 0.1mm. The micro gripper consists of a piezoelectric actuator, a displacement amplification mechanism, a flexible multi-stable structure, a clamp and a base. The left side is the amplification mechanism, which includes a lever mechanism and a parallelogram mechanism. On the right is a flexible multi stable mechanism, which includes three bistable mechanisms. The clamp arm is directly connected to the fixed base through a parallelogram mechanism, isolating parasitic deflection motion and ensuring that the output of the micro clamp end is pure parallel motion.

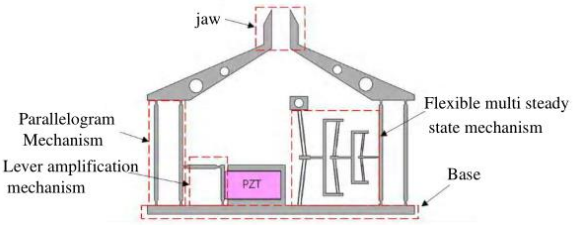

Figure 1 Structure diagram of micro clamp.

The working principle of this micro clamp is that the clamp mouth is in a normally open state, and the input end uses stacked piezoelectric ceramics (PZT) as the actuator. The clamping and releasing actions are achieved through the telescopic motion of the piezoelectric actuator. When applying voltage to the piezoelectric actuator, a driving displacement is generated at the input end of the micro clamp. One end of the PZT is fixed and the other end is connected to the lever mechanism. The input displacement of the piezoelectric actuator is first amplified by the lever mechanism in the first stage, and then transmitted to the parallelogram mechanism to ensure jaw translational motion and second stage amplification. Three flexible bistable mechanisms are connected in series on the right side to achieve eight steady states, Finally, the displacement is transmitted to the parallelogram mechanism to achieve jaw translation and amplification.

3. Micro clamp amplification mechanism

3.1 Structural design of amplification mechanism

The simplified schematic diagram of the enlarged mechanism is shown in Figure 3. At point A, the driving displacement P_{in} generated by the piezoelectric actuator is input, and the first stage amplification is achieved through the lever amplification mechanism. Then, the second stage amplification is achieved through the transmission of the parallelogram mechanism, ensuring that the end of the micro clamp moves purely parallel.

Finally, the output displacement X_{out} of the entire amplification mechanism is obtained at point F. l_1 is the distance from the input end of the lever amplification mechanism to the fixed end B, l_2 is the distance from the output end C of the first level lever mechanism to the fixed end B, l_3 and l_4 are the distances from the input end D and output end F of the second level lever to the fixed end E, respectively. The first level lever and the second level parallelogram mechanism rotate around the center axis of the flexible hinges H_1 and H_3, respectively. The above parameters are set as follows: $l_1 = 394.5\mu m$, $l_2 = 789\mu m$, $l_3 = 710\mu m$, $l_4 = 1339\mu m$.

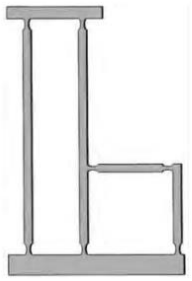

Figure 2 Leverage structure diagram.

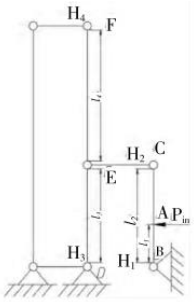

Figure 3 Simplified schematic diagram of lever structure.

3.2 Determination of Amplification Factor for Amplification Mechanism

During the motion of the amplification mechanism, under the action of force, the flexible hinge will simultaneously generate tension, compression, and angular deformation, resulting in drift of the rotation center of the flexible hinge, causing changes in the amplification coefficient of the lever amplification mechanism and the entire micro clamp. Therefore, in the study of lever amplification mechanism theory, it is necessary to consider the influence of the drift of the flexible hinge rotation center on the amplification coefficient. The axial force acting on the flexible hinge H_i is F_i, the torque is M_i, the rotation angle of the flexible hinge H_i around its central axis is θ_i, the axial deformation is Δ_i, the angle of the first lever ABC in the lever amplification mechanism is φ_1, the angle of the transition rod CE between the first lever ABC and the second lever DEF is φ_2, and the angle of the second lever DEF is φ_3.

The input displacement of the lever mechanism is the output displacement P_{in} of the piezoelectric actuator, which is:

$$X_A = P_{in} = X \tag{Eq.1}$$

The schematic diagram of the force on the BC rod is shown in Figure 4, which shows:

$$F_B + F_C = F_A \tag{Eq.2}$$

$$M_B + M_C + F_A l_1 = M_A + F_C l_2 \tag{Eq.3}$$

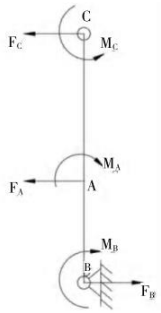

Figure 4 Schematic diagram of force on BC rod.

Hinge B undergoes compression under axial force, with a compression displacement of Δ_B. Therefore, the effective output displacement after passing through flexible hinge B is:

$$\varphi_1 = \theta_B = \frac{X_A}{l_1} = \frac{X_C + \Delta_B}{l_2} \quad \text{(Eq.4)}$$

Where: $\Delta_B = F_B \bullet C_{x,F_x}, \theta_B = M_B \bullet C_{\theta,M_x}$

Based on the above, the output displacement of the first level lever is:

$$X_C = \frac{X_A}{l_1} l_2 - \Delta_B = \frac{X}{l_1} l_2 - \Delta_B \quad \text{(Eq.5)}$$

The schematic diagram of the force acting on the rod CE between the first and second level levers is shown in Figure 5. Based on its deformation, it can be concluded that:

$$F_C = F_E \quad \text{(Eq.6)}$$

$$M_C = M_E \quad \text{(Eq.7)}$$

$$\varphi_2 = \varphi_1 \quad \text{(Eq.8)}$$

The hinge H_2 is compressed by axial force, and the compression displacement is Δ_C. Therefore, the effective output displacement of the first level lever after passing through the flexible hinge H_2 is:

$$X_E = X_C - \Delta_C = \frac{X}{l_1} l_2 - \Delta_B - \Delta_C \quad \text{(Eq.9)}$$

$$\Delta_C = F_C \bullet C_{x,F_x} \quad \text{(Eq.10)}$$

The force diagram of the parallelogram mechanism is shown in Figure 6. Based on its force analysis, it can be concluded that:

$$F_E = F_D \quad \text{(Eq.11)}$$

$$M_E = M_D + F_C l_4 \quad \text{(Eq.12)}$$

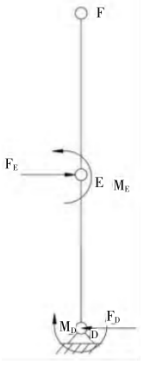

Figure 5 Schematic diagram of force on rod CE. **Figure 6** Schematic diagram of force on rod DEF.

The input end of the parallelogram mechanism is point E, and the hinge H_3 will be compressed under axial force, with a compression amount of Δ_3; At the same time, the hinge H_3 rotates around the center of rotation, with a rotation angle of φ_3, resulting in:

$$\varphi_3 = \theta_D = \frac{X_E - \Delta_D}{l_3} = \frac{X_F - \Delta_D}{l_3 + l_4} \quad \text{(Eq.13)}$$

$$\Delta_D = F_D \bullet C_{x,F_x} \quad \text{(Eq.14)}$$

$$\theta_D = M_D \bullet C_{\theta,M_x} \quad \text{(Eq.15)}$$

Overall, the effective output displacement of the entire amplification mechanism is:

$$X_{total} = X_F \frac{X_E - \Delta_D}{l_3}(l_3 + l_4) + \Delta_D = \frac{\frac{X}{l_1} l_2 - \Delta_B - \Delta_C - \Delta_D}{l_3}(l_3 + l_4) + \Delta_D \quad \text{(Eq.16)}$$

The magnification of the entire amplification mechanism is:

$$K = \frac{X_{total}}{X} = \frac{\frac{X}{l_1} l_2 - \Delta_B - \Delta_C - \Delta_D}{X l_3}(l_3 + l_4) + \frac{\Delta_D}{X} \quad \text{(Eq.17)}$$

Substitute specific data, $K = 4.52$.

3.3 Simulation Analysis of Amplification Mechanism

Based on the amplification factor of the amplification mechanism derived above, finite element analysis will be used to verify these formulas. Establish a finite element simulation model based on the geometric model shown in Figure 2, and analyze the motion range and stress situation of the amplification mechanism. Apply a displacement of 120 μm at the input end of the amplification mechanism, as shown in Figure 7, with a maximum output displacement of 499.78 μm.

The amplification factor of the left amplification mechanism was determined to be 4.16 through finite element simulation, while the theoretical model calculated the amplification factor to be 4.52, with an error of 8.6% compared to the finite element simulation results.

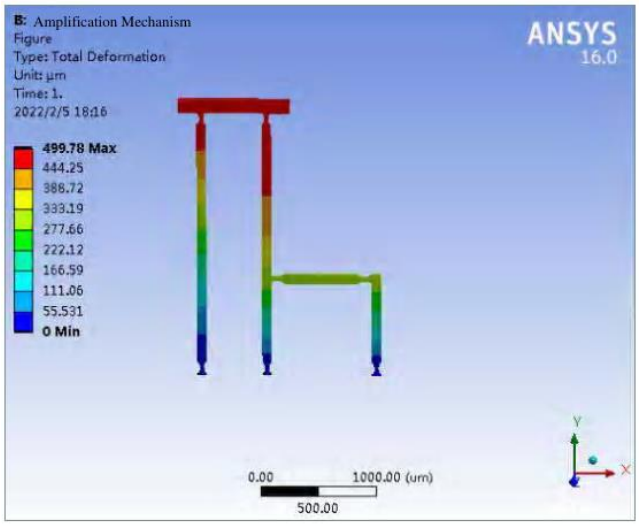

Figure 7 Enlarged displacement diagram of the mechanism.

4. Design and Simulation Analysis of Multi Steady State Structures

4.1 Theoretical Analysis of Single Bistable State

In order to gain a deeper understanding of the effects of different parameters on the bistable stability characteristics and select the most suitable design parameters for controlling the multi steady state performance, a single compliant bistable model is first analyzed, as shown in Figure 8. The initial state of the bistable state is bending, with a length of L, a rectangular cross-sectional area of $A = b \times d$, and a second-order moment $I_{yy} = bd^3/12$. The initial state of the bistable state can be represented by the function $Z_0(x) = h\varphi(x)$, where h is the height from the center point of the bistable state to the initial position, and $\varphi(x)$ is a dimensionless function $\max_{<0X<1}\{\varphi(x)\} = 1$.

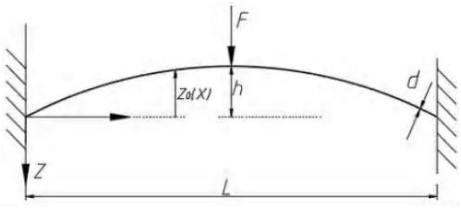

Figure 8 Single compliant bistable model.

After analysis, it was found that:

$$\varphi_0(x)=\frac{1}{2}-\frac{1}{8}\left(\frac{L}{h}\right)^2+\frac{1}{2}\sqrt{\left(1+\left(\frac{L}{2h}\right)^2\right)^2-\left(\frac{L}{h}\right)^2\left(\frac{2X}{L}-1\right)^2} \quad \text{(Eq.18)}$$

The initial processing state of the bistable state is a curved shape, so the beam is stress free in its initial bending state. Assuming that the beam is made of an isotropic homogeneous linear elastic material with a Young's modulus of E, with both ends fixed and driven by a concentrated force F acting on the midpoint of the beam in the Z-direction, as shown in Figure 8.

Firstly, the theoretical model of the beam is established using the Euler Bernoulli theory, which facilitates the adjustment of the preliminary design parameters for bistability. In addition, the theoretical results of the model will be used for comparison with the finite element results. Assuming $d \ll L, h \ll L$, the displacement equation of the beam can be described by two sets of differential equations:

$$EA\left[u'-h\varphi_0'w'+\frac{1}{2}(w')^2\right]'=0 \quad \text{(Eq.19)}$$

$$EIw^{IV}+EA\left[\left(h\varphi_0'-w'\right)\left(u'-h\varphi_0'w'+\frac{1}{2}(w')^2\right)\right]'=F\delta\left(X-\frac{L}{2}\right) \quad \text{(Eq.20)}$$

Where $w(x)$ is the lateral displacement; $u(x)$ is the axial displacement, and $\delta(x)$ is the Dirac function. Equation (19) is derived from the boundary conditions fixed at both ends of the beam. Two identical beams form a bistable structure through rigid connections, therefore it is symmetrical with a boundary condition $w'=0, EI_{yy}W'''=F/2$ at the midpoint of the beam.

The equation system of Eq.(20) was numerically solved based on the collocation method[9], using the two-point boundary value problem solver $bvp4c$ integrated into the Matlab package[10]. The system of Eq. (20) is written in the form of six first-order differential equations:

$$y'=f(y,F) \quad \text{(Eq.21)}$$

Where $y=\{u,u',w,w',w'',w'''\}^T$ is a vector of unknown parameters, and F is the force applied to the bistable state.

4.2 Multi Steady State Structural Design

Based on the above theory, the relationship between the lateral displacement $w(x)$ and the structural parameters in the bistable jump displacement equation can be obtained. Therefore, a bistable structure was designed, with the parameters shown in Table 1. Figure 9 shows the important variables in parameterized design, where L represents the length of the rigid rod, W represents the width of the rigid rod, β represents the angle of the rod, T represents the thickness, SW and SL represent the width and length of the shuttle, Y represents the displacement of the driving shuttle, and the material selected is aluminum alloy. Its Young's modulus (EX) is 71 GPa, and Poisson's ratio (PR) is 0.33. The bistable mechanism relies on the deflection of the compliant rod to move to its alternating stable position.

Table 1 Design Parameter Values of Three-Stage Compliant Bistable Mechanism.

L_1	L_2	L_3	W_1	W_2	β_1	β_2	β_3	Y	T
114.6 μm	252.6 μm	151.4 μm	5.0 μm	10.4 μm	6.6°	6.6°	6.6°	115.8 μm	7.0 μm

The bistable mechanism has two distinct stable equilibrium positions, and Figure 10 shows the force displacement relationship curve of the compliant bistable mechanism obtained through nonlinear finite element analysis. The point A and point C on the force displacement characteristic curve represent two steady-state positions (point A represents the initial position), while point B is a non-stationary position.

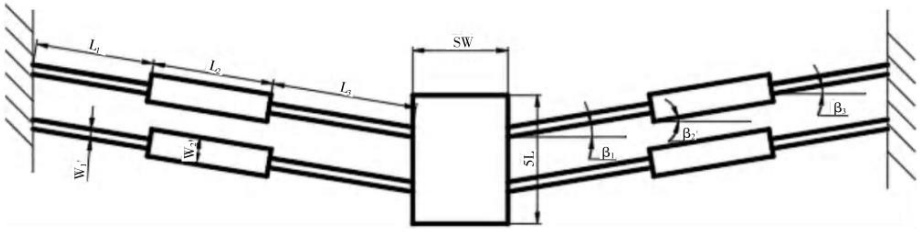

Figure 9 Structural schematic diagram of bistable mechanism.

F_{max} is the force applied by the bistable state to jump from the first steady-state position to the second steady-state position, while F_{min} is the force applied by it to jump from the second steady-state position to the first steady-state position. Between point A and point C is the bistable characteristic segment, within which the compliant bistable mechanism jumps from the initial position A through the non steady state position B to the second steady state position C.

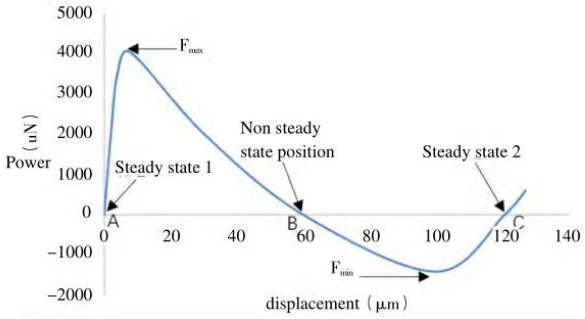

Figure 10 Force displacement curve of compliant bistable mechanism.

Multiple compliant bistable mechanisms are connected in series to achieve multi-stable functionality, with each bistable connected to a rigid frame, as shown in Figure 11. Name the bistable state from left to right as bistable state 1, bistable state 2, and bistable state 3, respectively. The required jumping force for each bistable state should be different, so a series of steady-state mutations will occur as the applied force continues to increase, as shown in Figure 12.

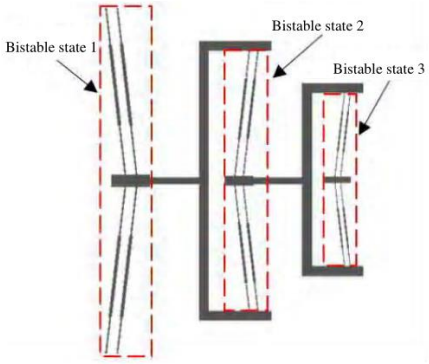

Figure 11 Multi steady state structure.

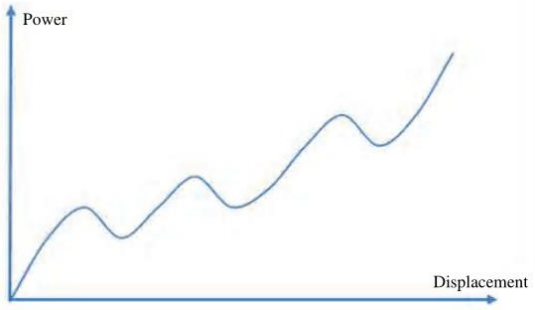

Figure 12 Multiple steady-state mutation curve.

4.3 Multi Steady State Simulation Analysis

The above multi steady state theoretical model will be verified through finite element simulation. Due to the similarity of these three bistable structures, only one bistable state 3 was simulated. This article selects aluminum alloy materials (which have a high ratio of yield strength to Young's modulus, allowing for a larger workspace for compliant mechanisms when material properties permit), with elastic modulus $E = 71GPa$, Poisson's ratio $PR = 0.33$, shear yield strength $\sigma = 275MPa$, and density $\rho = 2770kg/m^3$.

The finite element simulation results are shown in Figures 13 and 14. From the graph, it can be seen that the span of bistable 3 is 115.8um, with a stress of 47.7 MPa, which does not exceed the maximum allowable stress of the material of 275 MPa.

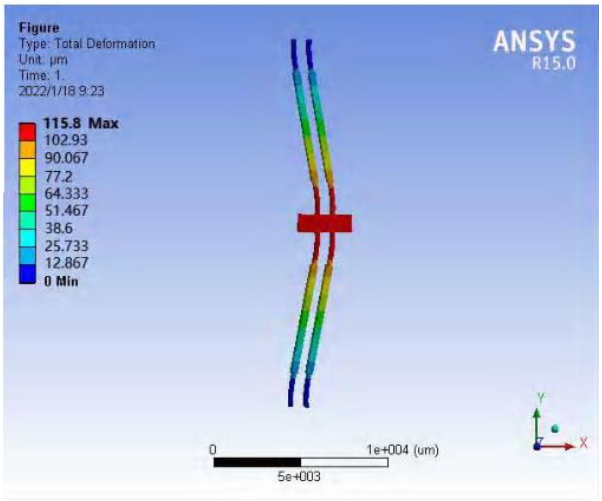

Figure 13 Bistable displacement diagram.

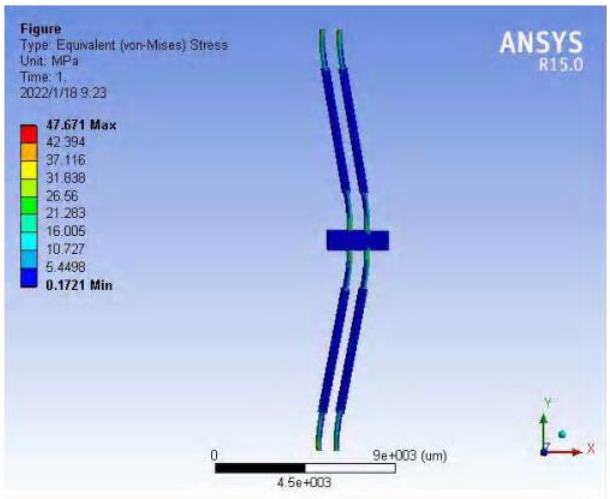

Figure 14 Bistable Stress Diagram.

From Figures 15 and 16, it can be seen that there is a sudden change in the displacement and stress of the bistable state, indicating that bistable state 3 has indeed achieved a jump. All simulation data for bistable systems are shown in Table 2.

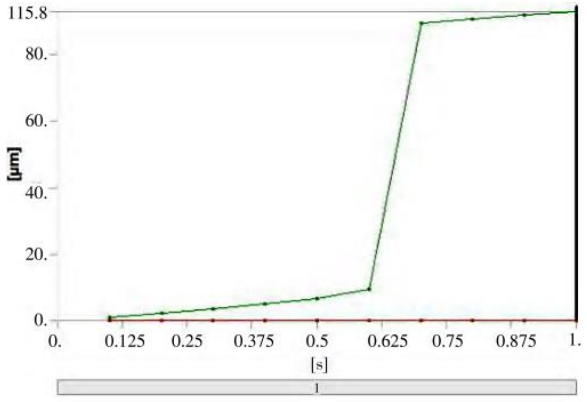

Figure 15 Bistable displacement curve.

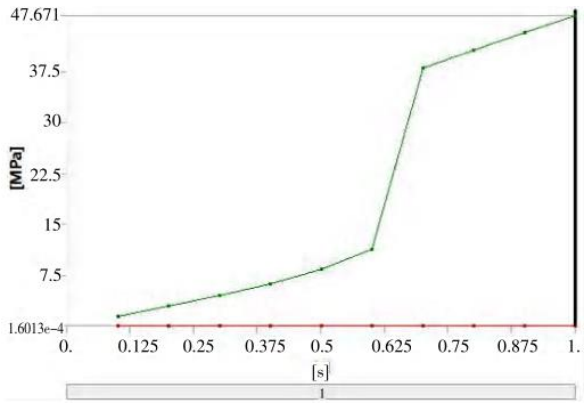

Figure 16 Bistable Stress Curve.

Table 2 Bistable Simulation Data.

	Displacement/ μ m	Stress/MPa	Applied force/ μ N
Bistable 1	248.51	90.2	8000
Bistable 2	186.4	65.8	6000
Bistable 3	115.8	47.7	4000

Next, the bistable states 1 and 2 will be simulated in series, and the results are shown in Figure 17. The

displacement is approximately equal to the sum of the individual displacements of the two bistable states.

Simulations were conducted by connecting bistable state 3 and parallelograms in series. The results are shown in Figure 18. After passing through the parallelograms, the displacement was amplified by about 2 times, which is consistent with the theoretical values.

The total displacement of multiple bistable and parallelogram structures is 1025.91um, which can meet the requirements of cross scale from micrometers to millimeters. The maximum stress is 200.91 *MPa* , which is lower than the maximum allowable stress of 275 *MPa* for aluminum alloy. Therefore, the designed multi steady state structure meets the requirements of micro clamps.

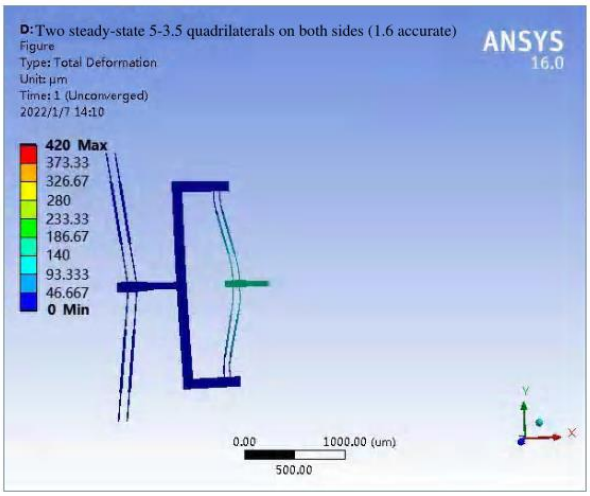

Figure 17 Two bistable series displacement diagrams.

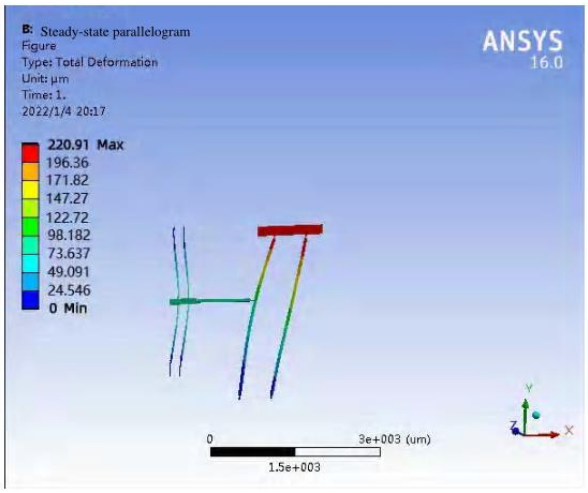

Figure 18 Series displacement diagram of bistable and parallelogram mechanisms.

5. Conclusion

This article designs a cross scale micro clamp based on a multi steady state compliant mechanism, which has the advantages of compact structure, large displacement range, and translational clamping, and can achieve cross scale micro operations from micrometers to millimeters. Theoretical analysis and design of the structure of the micro gripper were conducted using a static mechanics model, and the performance of the micro gripper was verified using finite element simulation analysis software. Compared with similar micro clamps, this micro clamp has good practical value.

Conflict of Interest

The authors declare no conflict of interest.

References

1. Zhang Peiyu, Wu Guoying, Hao Yilong, Li Zhijun. Progress and prospects of micro clamp research [J]. Optical Precision Engineering, 2000 (03): 292-296.
2. Wang Xiaodong, Liu Chong, Wang Liding. The latest research on micro clamps [J]. Journal of Functional Materials and Devices, 2004 (01): 1-8.
3. Yang Qun, Jin Baomin, Xu Xiaohui. Design and analysis of a micro clamp compliant mechanism [J]. Ship Chemical Protection, 2012 (01): 15-20.
4. Lu Quanguo, Zeng Bin, Tang Gang. Structural design and optimization of a micro clamp body [J]. Mechanical Design and Research, 2015, 31 (01): 48-50.
5. Li Jiajie, Chen Guimin. Optimization design of flexible two-stage differential micro displacement amplification mechanism [J]. Journal of Mechanical Engineering, 2019, 55 (21): 21-28.

6. Yanru Zhao,Xiaojie Huang,Yong Liu,Geng Wang,Kunpeng Hong. Design and Control of a Piezoelectric - Driven Microgripper Perceiving Displacement and Gripping Force [J]. Micromachines, 2020,11(2).
7. Ding Yan, Lai Leijie. Structural design of flexible piezoelectric micro clamps with large stroke and no parasitic displacement [J]. Piezoelectricity and Acousto Optics, 2019, 41 (04): 562-565.
8. Chen Xiaodong, Deng Zilong, Xingxin Jun. Design of Asymmetric Piezoelectric Microclamp Based on Hinge Stiffness [J]. Sensors and Microsystems, 2020, 39 (06): 66-69.
9. L. Shampine, A BVP solver based on residual control and the MATLAB PSE, ACM Trans. Math. Software 27 (2001): 299-316.
10. L. Shampine, M.W. Reichelt, J. Kierzenka, Solving Boundary Value Problems for Ordinary Differential Equations in MATLAB with bvp4c, Available at:/www.mathworkscom/bvp tutorialS.